Supplement of

Large-eddy simulation and stochastic modelling of Lagrangian particles for footprint determination in stable boundary layer

Andrey Glazunov[1], Üllar Rannik[2], Victor Stepanenko[3], Vasily Lykosov[1,3], Mikko Auvinen[2], Timo Vesala[2], and Ivan Mammarella[2]

[1]Institute of Numerical Mathematics RAS , GSP-1, 119991, Gubkina str., 8, Moscow, Russia
[2]Department of Physics, P.O. Box 64, University of Helsinki, 00014 Helsinki, Finland
[3]Moscow State University, Research Computing Center, GSP-1, 119234, Leninskie Gory, 1, bld. 4, Moscow, Russia

Correspondence to: A. Glazunov (and.glas@gmail.com)

S1 The comparison of Lagrangian particles transport in LES with measurements under convective and shear-convective conditions

Below we present the LES results of Lagrangian particles transport in a purely convective boundary layer (with a very small absolute value of the Obukhov scale L) and in a shear-convective boundary layer, where the roles of wind shear and buoyancy are comparable. The approach based on velocity "defiltering" was used. Stochastic subgrid model was applied only within the nearest to the surface computational layer. The interpolation of mean velocity into a particle position inside the layer $z < \Delta_g$ was performed taking into account the appropriate universal functions (Businger et al., 1971). First the correctness of the particles advection with the use of very rough grids was evaluated.

S1.1 Convective conditions

The crosswind integrated concentration (CWIC) of the particles emitted from the elevated source:

$$C^y(x',z,z_s) = Q\left\langle \int_{-\infty}^{\infty}\int_{0}^{\infty} p(x',y',z,t'|x_s,y_s,z_s)dt'dy' \right\rangle_{x_s,y_s},$$

was compared with the laboratory data obtained in (Willis and Deardorff, 1976). Here Q denotes the source strength; t' - time interval between the ejection and detection; (x_s, y_s, z_s) - position of the source; $x' = x - x_s$ and $y' = y - y_s$ - distances from the source in wind and crosswind directions, correspondingly; p -particle position PDF.

The setup of numerical experiments was close to that presented in (Weil et al., 2004) and
(Steinfeld et al., 2008). The convective layer of height $z_i = 1000$ m was simulated under the strong unstable conditions $L/(\kappa z_i) \approx -0.01$. The particles were emitted at the altitude $z_s = 0.07 z_i$.

The LES runs were performed with grids steps $\Delta_g = 10$ m $\approx z_i/100$, $\Delta_g = 20$ m $\approx z_i/50$, $\Delta_g = 40$ m $\approx z_i/25$ and $\Delta_g = 80$ m $\approx z_i/12$ (equidistant grids were used $\Delta_x = \Delta_y = \Delta_z$). The last two grids are sufficiently rough to provide substantial impact of subgrid processes in this flow. Note that the source is placed within the second computational layer for the grid with $\Delta_g = 40$ m and within the first one if $\Delta_g = 80$ m.

The results in comparison to laboratory data (Willis and Deardorff, 1976) are shown in Fig. S1.1. The normalized CWIC $\tilde{C}^y = C^y U z_i/Q$ depending on nondimensional height z/z_i and on the nondimensional distance from the source $X = (x - x_s)w^*/(U z_i)$ is displayed, where U denotes the averaged velocity in convective zone (from 0 to z_i), w^* is the convective velocity scale. Fig. S1.1a shows that significant differences from measurements were obtained with the grid steps $\Delta_g \approx z_i/12$. Note that this step is too rough to reproduce correctly the Eulerian velocity in LES. Within the range $(z_i/25 \le \Delta_g \le z_i/100$ the concentration $\tilde{C}^y$ near the source of emission is reproduced almost independently on the grid size and corresponds to the observation data. One can see some differences between the curves near the upper boundary of the convective layer. These errors are mostly connected with poorly resolved

entrainment layer and with the wrong Eulerian dynamics computed at very rough grids.

Fig. S1.1b shows CWIC isolines, computed with $\Delta_g = 10$ m (upper panel) and $\Delta_g = 40$ m (lower panel). One can see, that it is possible to get qualitatively realistic concentration transport even in those cases when the source altitude z_s (here $z_s = 70$ m) is comparable with the grid step.

S1.2 Shear-convective conditions

Scalar fluxes footprints in shear-convective ABL were studied earlier in (Steinfeld et al., 2008) and (Leclerc et al., 1997). There, the LES results were compared with the tracer field observations data (Finn et al., 1996). Below are the results of calculations corresponding to the case (b) from (Leclerc et al., 1997) (Obukhov length $L/\kappa \approx -32$ m, boundary layer height $z_i \approx 500$ m, friction velocity $U_* \approx 0.28$ m/s). The setups of experiments were as follows: initial ABL height $z_i = 500$ m; initial potential temperature $\Theta = 300$ K if $z \le z_i$ and $d\Theta/dz = 0.01$ K/m if $z > z_i$; initial wind velocity magnitude $U(z, t = 0) = U_g$ =4.5 m/s; this velocity has been turned 24° clockwise with respect to x-axis. Surface temperature flux was set to 0.05 Km/s. Roughness parameter z_0 was set to 0.14 m. Large scale negative velocity $W_d(z) = -0.014(z/z_i)$ m/s was added to compensate the growth of boundary layer. The simulations were performed in periodic rectangular domain of $2 \times 2 \times 1$ km^3 size. The time of each simulation was not less than 5 hours. Particles were emitted at the height $z_s = 0.75$ m starting at time $t_s = 3$ h with the rate of one particle in each near-wall grid cell per the time interval $\Delta t_{ej} = 16$ s. The grid steps were Δ_g=5, 10, 20 and 40 meters.

Figure S1.2a,b shows the Obukhov lengths L/κ and the friction velocities U_* computed with different resolutions. In all cases, the required values ($L/\kappa \approx -32$ m, $U_* \approx 0.28$ m/s) were achieved approximately after four hours of simulations. Time interval $\{t_i, t_e\}$ (see Fig.S1.2a) between the fourth and firth hours was used for averaging and the footprints evaluation. The mean wind velocity and the variances of the "defiltered" wind velocity components are shown in Fig. S1.2 c,d. The mean velocity is nearly the same in different simulations and is directed along x-axis. In the simulations with the rough grids the variance of longitudinal velocity is underestimated, but the vertical variance is less sensitive to resolution.

The computed one-dimensional crosswind-integrated footprints f_s^y and the correspondent cumulative footprints F for the sensor heights $z_M = 10$ m and $z_M = 100$ m are shown in Fig. S1.3. Symbols in Fig. S1.3 a,b denote the observation data obtained in (Leclerc et al., 1997) (note, that cumulative footprint F can not be measured directly if the number of sensors is limited, so the estimate of this value is shown). Significant differences between the data and the simulation results were obtained with the roughest grid only. This result is satisfactory, taking into account that at the resolutions Δ_g=20 and 40 meters footprints were calculated for the sensors located inside the first grid cell.

Similar simulations with the LES model PALM (see, Fig. 4 in Steinfeld et al., 2008) showed the strong sensitivity of results to the spatial resolution regardless if the subgrid stochastic modelling was used or not.

For the sensor height $z_M = 100$ m the dependence of the functions f_s^y and F on the grid spacing is weak (see Fig. S1.3c,d). Some differences in cumulative footprints F at large distances $x_M - x$ (see Fig. S1.3d) are not systematic with respect to the grid size and can be attributed to insufficient statistical precision of the large eddies averaging (see, for example, (Cai et al., 2010)).

S2 Footprint simulations above the heterogenous surface

The setup of numerical experiment discussed in this section is identical to that presented in
(Glazunov and Stepanenko, 2015). The turbulent flow above the "lake" , surrounded by the "forest" was considered. The "lake" was prescribed as an ellipse with semiaxes 200m and 60m. The effect of trees was taken into account by using an array of simple objects (rectangular parallelepipeds) with the height $h = 16$ m that provides the displacement height $D \approx 14$ m and the roughness parameter $z_0 \approx 0.55$ m characteristic for a forest canopy. The simulations were conducted in a non-periodic domain with the turbulent inflow generated by an additional LES model with periodic domain. The simulations were performed with the grid step $\Delta_g = 1$m. Mesh size was $512 \times 256 \times 64$ grid points. The mean velocity at the height $2h$ was approximately 3.5 m/s. One can find more detailed description in (Glazunov and Stepanenko, 2015).

Simulations with the Lagrangian particles were performed for the case of unstable stratification above the "lake" and with the wind directed along the main ellipse axis. Two simulations have been performed with durations of 0.5 hour. The last twenty minutes of each simulation were used for footprints calculation.

The particles were emitted at the height 0.1 m with the time intervals $\Delta_{ej}^p = 0.025$ sec within each grid cell near the surface. Rectangular areas $x_M^k - \Delta_a < x < x_M^k + \Delta_a$, $y_M^k - \Delta_a < y < y_M^k + \Delta_a$ with the size $S_M = 4 \times 4$ m^2 surrounding sensor positions were selected. Footprints were accumulated on the grid with the cells of $S_S = 1 \times 1$ m^2.

Figure S2.1a shows the total number of particles N_{p-tot} residing in computational domain simultaneously depending on the simulation time. The number of particle is stabilized near the value $\sim 0.9 \times 10^9$ due to absorbtion condition in outflow. The total number of the particles emitted in each simulation was approximately 7.5×10^{10}.

Figure S2.1b shows the instant numbers of particles in each grid cell (third computational level above the surface). The particle concentration is variable in space due to tur-

bulent character of the flow. One can see, that the significant part of the variance can be attributed to large-scale eddies. This leads to nonuniform loading of processors for parallel computing. In this calculation, performed with the two-dimensional domain MPI-decomposition at 256 nodes, the ratio of the maximum of the particles number per one node to the average number of particles in a subdomain is $n_{max}/n_{avr} \approx 2$ (see Fig. S2.1c). So the efficiency of the use of parallel resources does not exceed 50%. Here, the calculations of Lagrangian particles consume about 75% of the total computation time.

Two-dimensional footprint functions $f_s(x - x_M, y - y_M, z_M)$ that were computed for the three sensor positions marked by 1, 2 and 3 in Fig. S2.1b are shown in Fig. S2.1c,d,e (here $z_M = 3$m). These footprints were determined with the use of the averaging of results of two independent realizations, denoted by f_s^1 and f_s^2, respectively. These independent experiments resulted in correlation $corr(f_s^1, f_s^2) \approx 0.97, 0.98$ and 0.98 and the normalized error with respect to mean value $\left\langle (f_s^i - f_s)^2 \right\rangle_{xy}^{1/2} / \left\langle (f_s)^2 \right\rangle_{xy}^{1/2} \approx 0.13$, 0.11 and 0.07, depending on the sensor points 1, 2 and 3, respectively. Thus, the developed technology allows to determine the footprints above inhomogeneous surfaces without the need for averaging over a large area. In this numerical experiment, due to intensive production of turbulence at the altitudes close to the "trees height" , the elongation of footprints appears to be small in comparison to the size of the "lake".

References

Businger, J. A., J. C. Wyngaard, Y. Izumi, and E. F. Bradley: Flux–profile relationships in the atmospheric surface layer. J. Atmos. Sci., 28, 2, 181–189, 1971.

Xuhui Cai , Jiayi Chen, Raymond L. Desjardins: Flux Footprints in the Convective Boundary Layer: Large-Eddy Simulation and Lagrangian Stochastic Modelling. Boundary-Layer Meteorol., 137, 1, 31–41, 2010.

Glazunov A.V. and Stepanenko V.M.: Large eddy simulation of stratified turbulent flows over heterogeneous landscapes. Izvestiya, Atmospheric and Oceanic Physics, 51, 4, 351–361, 2015.

Finn, D., Lamb, B., Leclerc, M.Y., Horst, T.W.: Experimental evaluation of analytical and Lagrangian surface-layer flux footprint models. Boundary-Layer Meteorol., 80, 283–308, 1996.

Leclerc, M. Y., Shen, S., Lamb, B.: Observations and large-eddy simulation modeling of footprints in the lower convective boundary layer. J. Geophys. Res. 102, 9323–9334, 1997.

Steinfeld G., Raasch S. and Markkanen T.: Footprints in Homogeneously and Heterogeneously Driven Boundary Layers Derived from a Lagrangian Stochastic Particle Model Embedded into Large-Eddy Simulation. Boundary-Layer Meteorol., 114, 3, 503–523, 2008.

Weil J. C., Sullivan P. P. and Moeng C-H.: The Use of Large-Eddy Simulations in Lagrangian Particle Dispersion Models. J. Atmos. Sci., 61, 23, 2877-2887, 2004.

Willis, G. E., and J. W. Deardorff: A laboratory model of diffusion into the convective planetary boundary layer. Quart. J. Roy. Meteor. Soc., 102, 427–445, 1976.

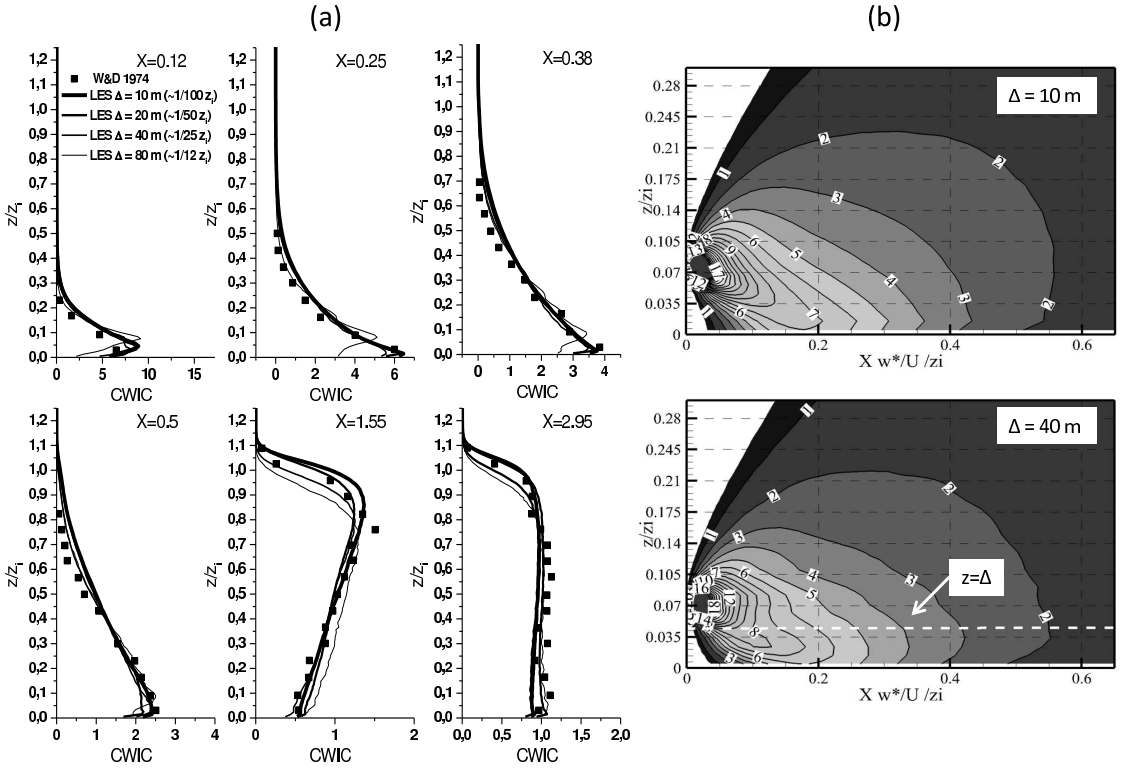

Figure S1.1. Crosswind integrated concentration $\tilde{C}^y = C^y U z_i/Q$ depending on normalized height z/z_i and non-dimensional distance from the source $X = xw^*/(Uz_i)$. (a) CWIC profiles $\tilde{C}^y$ computed in LES with different resolution (solid lines) in comparison with laboratory data (squares). (b) CWIC isolines computed with grid steps $\Delta_g = 10$ m$\approx z_i/100$ and $\Delta_g = 40$ m$\approx z_i/25$ (dashed line - first computational level $z = \Delta_g$).

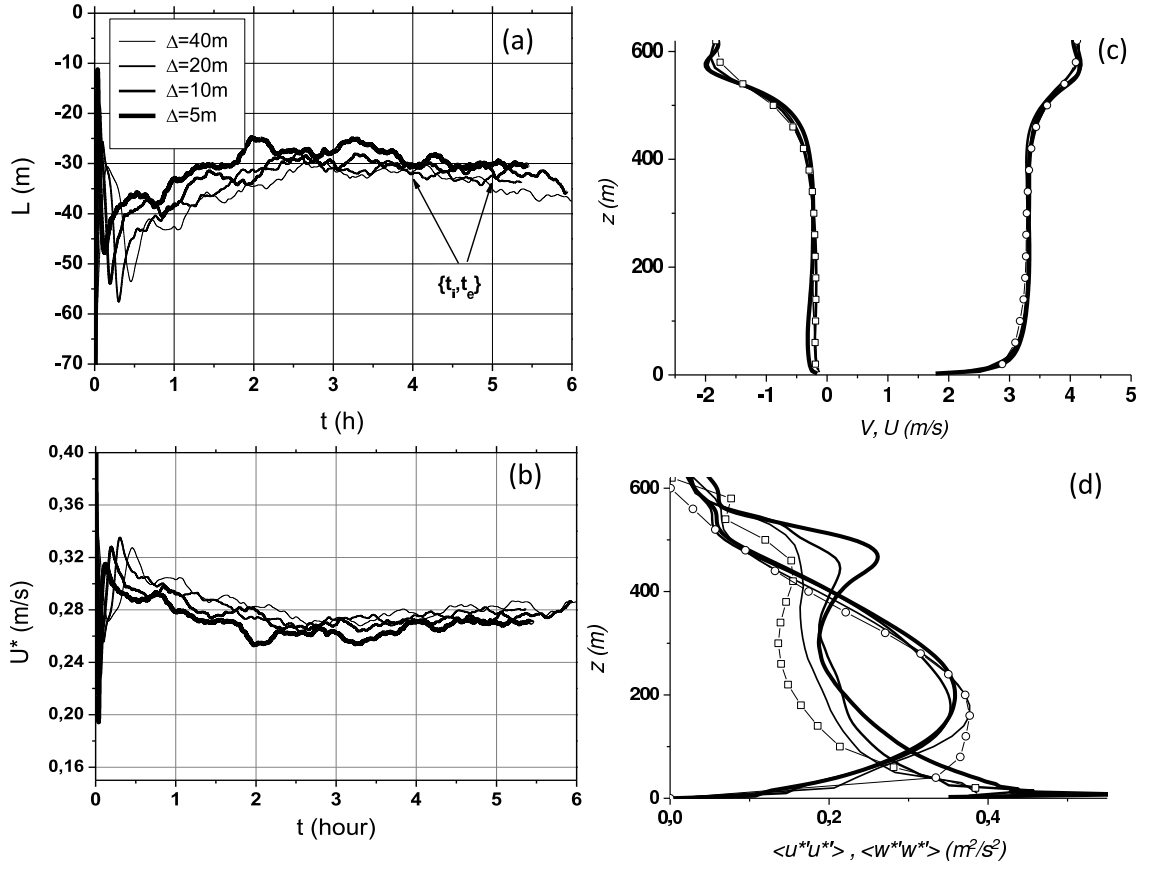

Figure S1.2. (a) Obukhov length L/κ, the time interval chosen for averaging $\{t_i, t_e\}$ is shown ; (b) friction velocity U_*; (c) mean wind velocity components; (d) variance of vertical velocity (marked by the circles for $\Delta_g = 40$ m) and variance of the longitudinal velocity (marked by the squares for $\Delta_g = 40$ m). The results are shown for the grid steps Δ_g=5, 10, 20 and 40 meters (the most thick line - Δ_g=5 m and the most thin line - Δ_g=40 m).

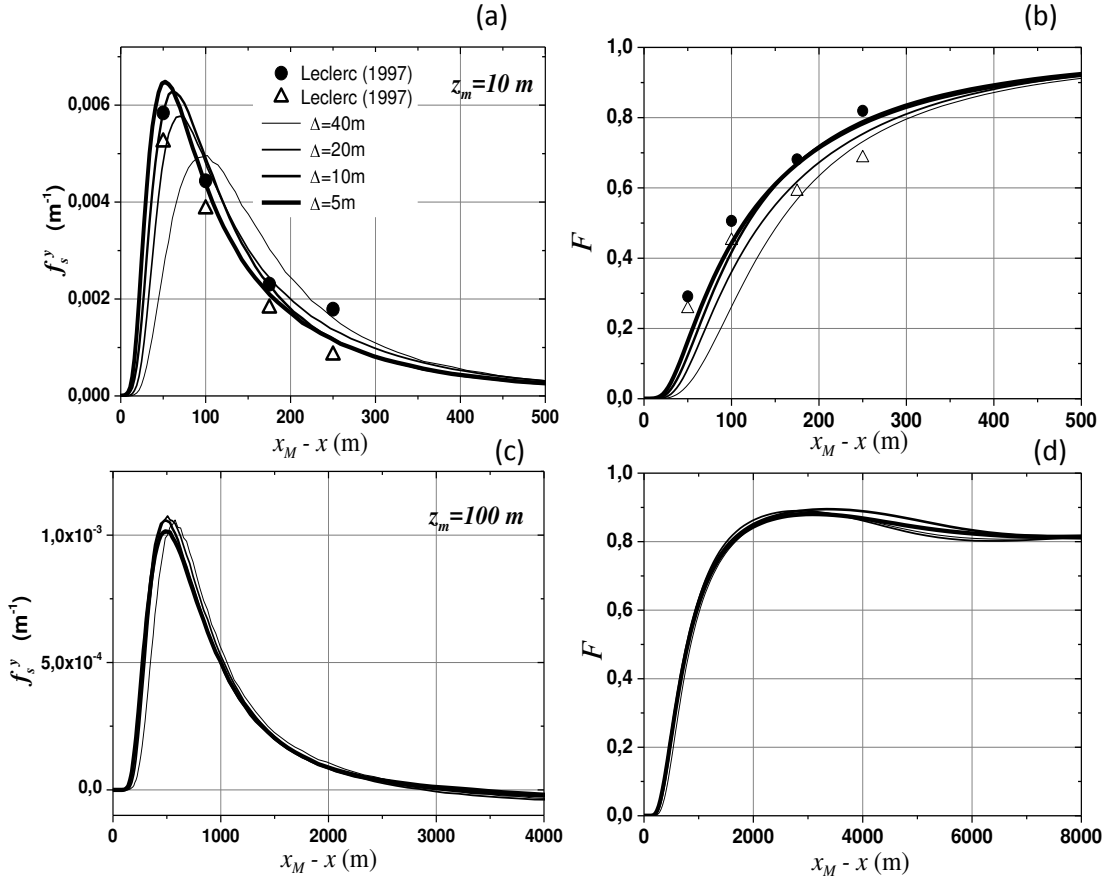

Figure S1.3. Footprints f_s^y (a,b) and cumulative footprints F (c,d) for the sensor heights z_M=10m (a,b) and z_M=100m (c,d), computed with the different spatial resolution in LES. Symbols - observational data (Leclerc et al., 1997)

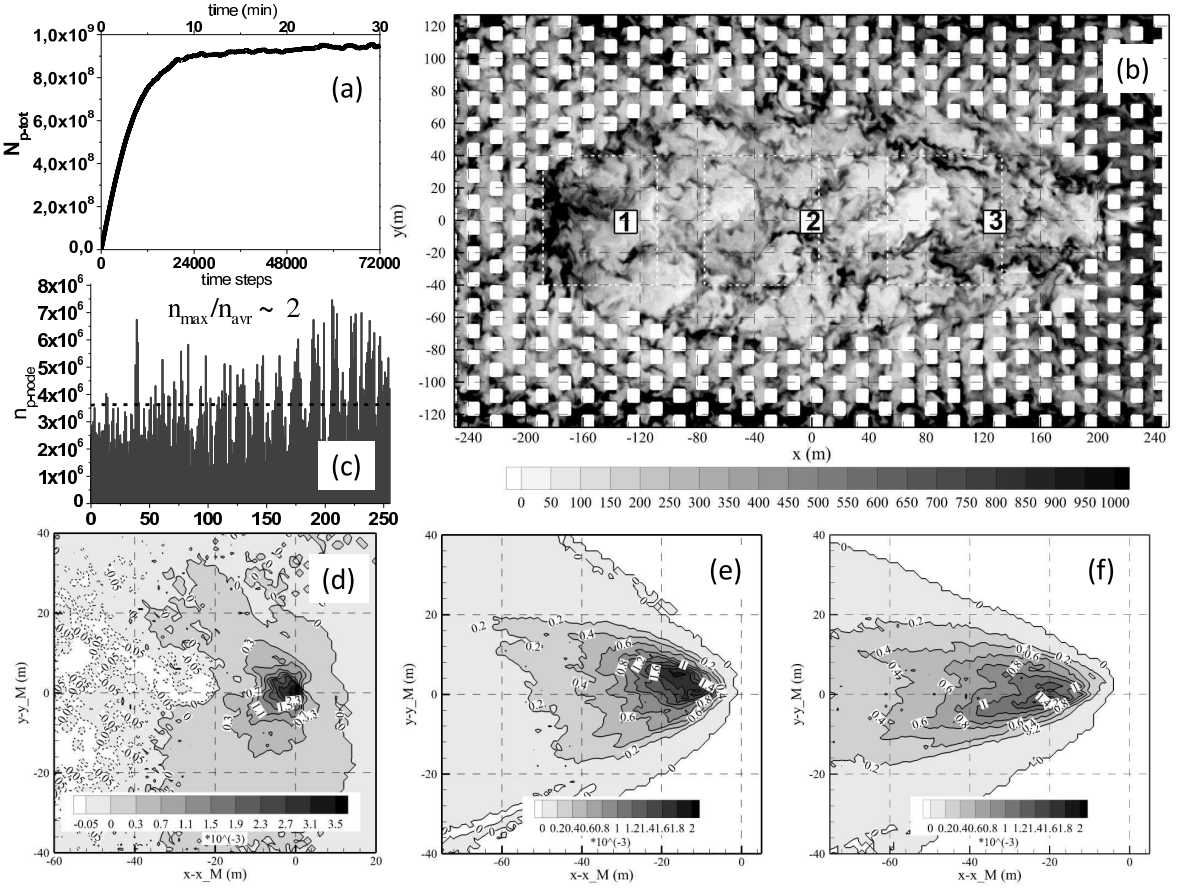

Figure S2.1. (a) Total number of the particles N_{p-tot} depending on the simulation time. (b) Instant numbers of the particles inside each grid cell (third level above the surface). (c) Numbers of the particles inside each parallel subdomain n_{p-node}. (d,e,f) Footprints $f_s(x - x_M, y - y_M, z_M)$ for the points marked by the numbers 1, 2 and 3 and squares in Fig. S2.1b for the sensor height $z_M = 3$ m.